

FERROMAGNETIC CYLINDERS IN EARTH'S MAGNETIC FIELD—A TWO-DIMENTIONAL MODEL OF MAGNETIZATION OF SUBMARINE

X. B. Xu and L. Zeng

Department of Electrical & Computer Engineering
Clemson University
Clemson, SC 29634-0915, USA

- 1. Introduction**
 - 2. Formulation of the Integral Equations**
 - 3. Numerical Solution Scheme**
 - 3.1 Results
 - 3.2 The Asymmetric Coupler
 - 4. Computation of Magnetic Field**
 - 4.1 Overlap Integrals
 - 5. Results and Discussion**
- References**

1. INTRODUCTION

A submarine, made of steel and magnetized in the earth's magnetic field, disturbs local magnetic field. Such a disturbance makes the submarine "visible" to magnetic field sensors. To reduce the probability of the submarine being detected and targeted, it is desired to minimize the field perturbation. This can be done by a proper placement of degaussing coils on the surface of the submarine. An optimal design of degaussing system relies on a thorough understanding of the magnetization of the submarine. It requires detailed information about the magnetization current induced on the surface of the submarine and the magnetic field produced by the surface magnetization current.

In the past, finite element method has been employed to model ship magnetization [1]. This method is accurate but is time-consuming

and requires a large computer memory since a large number of meshes are needed to model a ship. It is well known that steel, which is used to make a submarine shell, is a nonlinear ferromagnetic material. Its permeability varies as a function of the magnetic field intensity. However, under the influence of the earth's magnetic field which is only on the order of 10^{-4} Wb/m² [2], the portion of the B-H curve of steel is approximately a straight line. Therefore, a constant permeability can be assumed for the whole submarine shell. Under this condition, boundary element method may be more suitable, comparing to finite element method, for treating the magnetization of a submarine, since less CPU time and computer storage are needed. To date, only a simple two-dimensional square box structure has been investigated using the boundary element method [3]. This box is assumed to be oriented in such a way that the external magnetic flux is parallel to its side walls. Obviously, a square box structure does not match the shape of a submarine. Also, the submarine may take any orientation relative to the earth's magnetic field, resulting in different magnetic signatures.

A three-dimensional (3-D) model of a submarine may best approximate its actual shape [4]. As a prelude to the 3D modeling, in this paper, we present a two-dimensional (2D) computational model, employing surface integral equation method, for the analysis of the magnetization of a submarine. The submarine is modeled as a two-dimensional (2D) magnetizable cylinder of infinite length placed in an external magnetic field. The cylinder may be of arbitrary cross section. However, special attention is given to circular and elliptic cylinders, whose cross sections are closest to that of a submarine. Realizing that the submarine may be randomly oriented relative to the earth's magnetic field, we decompose the earth's magnetic field into two components: one is perpendicular and the other is parallel to the cylinder axis. The effect of each of these two components is considered separately in this paper. Integral equation is formulated and the method of moments [5] is employed to solve for the unknown magnetization current on the cylinder surface. Based on knowledge of the magnetization current, the magnetic field created by the cylinder is calculated. Numerical results of the magnetization current and the resulting magnetic field are presented and discussed.

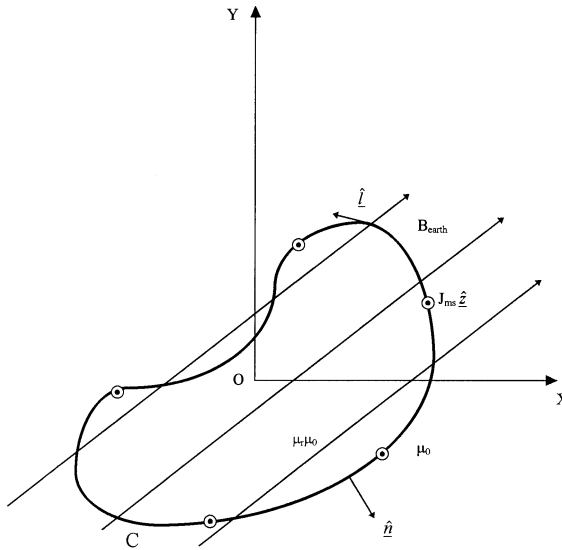


Figure 1. Cross section of a cylinder with earth's magnetic field perpendicular to its axis.

2. FORMULATION OF INTEGRAL EQUATION

In Fig. 1 is shown in cross sectional view a magnetizable cylinder, the axis of which is perpendicular to the earth's magnetic field. The other possible case is that the cylinder axis is parallel to the earth's magnetic field, which is illustrated in Fig. 2. The permeability of the cylinder is $\mu_r \mu_0$, and the permeability of the medium surrounding the cylinder is μ_0 . The coordinate system is set up in such a way that the z -axis coincides with the cylinder axis. The cylinder is magnetized and a magnetization current \vec{J}_{ms} is induced on the surface of the cylinder. The magnetization current \vec{J}_{ms} , in turn, generates a magnetic flux density \vec{B}_s that is found to be

$$\vec{B}_s = \nabla \times \oint_C \vec{J}_{ms}(\vec{\rho}') \mu_0 G(\vec{\rho}, \vec{\rho}') dl' \tag{1}$$

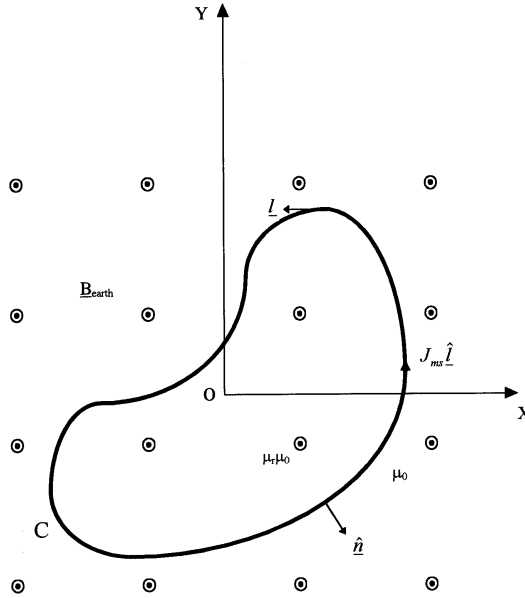


Figure 2. Cross section of a cylinder with earth’s magnetic field parallel to its axis.

where C is the bounding contour of the cylinder and $\vec{\rho}, \vec{\rho}'$ locate the field and source point. The 2D static Green’s function $G(\vec{\rho}, \vec{\rho}')$ is given by [6]

$$G(\vec{\rho}, \vec{\rho}') = -\frac{1}{2\pi} \ln |\vec{\rho} - \vec{\rho}'| + \frac{1}{2\pi} \ln |\vec{\rho}_R - \vec{\rho}'| \tag{2}$$

in which $\vec{\rho}_R$ locates a reference point at which $G(\vec{\rho}, \vec{\rho}')$ vanishes.

Note that the total magnetic field everywhere can be expressed as the sum of the earth’s magnetic field and the field produced by the magnetization current. Also, note that the tangential component of the total magnetic field intensity on the surface of the cylinder must be continuous since there is no free current. Enforcing this boundary condition requirement, one obtains

$$\begin{aligned} & \frac{1}{\mu_r \mu_0} \left[\hat{n} \times \vec{B}_e - \lim_{\vec{\rho} \uparrow C} \hat{n} \times \oint_C \vec{J}_{ms}(\vec{\rho}') \times \mu_0 \nabla G(\vec{\rho}, \vec{\rho}') dl \right] \\ & = \frac{1}{\mu_0} \left[\hat{n} \times \vec{B}_e - \lim_{\vec{\rho} \downarrow C} \hat{n} \times \oint_C \vec{J}_{ms}(\vec{\rho}') \times \mu_0 \nabla G(\vec{\rho}, \vec{\rho}') dl \right] \end{aligned} \quad \vec{\rho} \in C \quad (3)$$

Equation (3) can be further simplified corresponding to each of the following two cases: the earth’s magnetic field is perpendicular and parallel to the cylinder axis.

(1) The magnetic field of the earth is *perpendicular* to the cylinder axis. Under this condition, a *z*-directed magnetization current is induced on the cylinder surface and equation (3) can be rewritten as

$$\begin{aligned} & \frac{1}{\mu_r} \hat{n} \times \vec{B}_e - \frac{\mu_0}{\mu_r} \lim_{\vec{\rho} \uparrow C} \oint_C \frac{\partial G(\vec{\rho}, \vec{\rho}')}{\partial n} \vec{J}_{ms}(\vec{\rho}') dl' \\ & = \hat{n} \times \vec{B}_e - \mu_0 \lim_{\vec{\rho} \downarrow C} \oint_C \frac{\partial G(\vec{\rho}, \vec{\rho}')}{\partial n} \vec{J}_{ms}(\vec{\rho}') dl' \end{aligned} \quad \vec{\rho} \in C \quad (4)$$

Taking dot product of \hat{z} on both sides of equation (4), one has

$$\begin{aligned} & \frac{1}{\mu_r} B_{e,l} - \frac{\mu_0}{\mu_r} \lim_{\vec{\rho} \uparrow C} \oint_C \frac{\partial G(\vec{\rho}, \vec{\rho}')}{\partial n} \vec{J}_{ms,z}(\vec{\rho}') dl' \\ & = B_{e,l} - \mu_0 \lim_{\vec{\rho} \downarrow C} \oint_C \frac{\partial G(\vec{\rho}, \vec{\rho}')}{\partial n} \vec{J}_{ms,z}(\vec{\rho}') dl' \end{aligned} \quad \vec{\rho} \in C \quad (5)$$

in which $B_{e,l}$ is the component of the earth’s magnetic flux density tangential to the cylinder surface. Further, one notices that

$$\frac{\partial G}{\partial n} = \hat{n} \cdot \nabla G(\vec{\rho}, \vec{\rho}') = \hat{n} \cdot \left(-\frac{1}{2\pi} \frac{\vec{\rho} - \vec{\rho}'}{|\vec{\rho} - \vec{\rho}'|^2} \right)$$

or

$$\frac{\partial G}{\partial n} = -\frac{1}{2\pi} \frac{\cos \theta}{|\vec{\rho} - \vec{\rho}'|} \quad (6)$$

in which

$$\cos \theta = \hat{n} \cdot \frac{\vec{\rho} - \vec{\rho}'}{|\vec{\rho} - \vec{\rho}'|} \quad (7)$$

Then, going through the normal limiting procedure [7], one arrives at

$$\begin{aligned} & \frac{1}{\mu_r} B_{e,l} - \frac{\mu_0}{\mu_r} \left[-\frac{1}{2\pi} \oint_C \vec{J}_{ms,z}(\vec{\rho}') \frac{\cos \theta}{|\vec{\rho} - \vec{\rho}'|} dl' + \frac{\vec{J}_{ms,z}(\vec{\rho})}{2} \right] \\ & = B_{e,l} - \mu_0 \left[-\frac{1}{2\pi} \oint_C \vec{J}_{ms,z}(\vec{\rho}') \frac{\cos \theta}{|\vec{\rho} - \vec{\rho}'|} dl' - \frac{\vec{J}_{ms,z}(\vec{\rho})}{2} \right] \end{aligned} \quad (8)$$

or

$$-\frac{\mu_0}{2\pi} \oint_C \vec{J}_{ms,z}(\vec{\rho}') \frac{\cos \theta}{|\vec{\rho} - \vec{\rho}'|} dl' - \frac{\mu_r + 1}{\mu_r - 1} \frac{\mu_0 \vec{J}_{ms,z}(\vec{\rho})}{2} = B_{e,l}(\vec{\rho}), \quad \vec{\rho} \in C \quad (8')$$

where $\cos \theta$ is defined in equation (7).

(2) The magnetic field of the earth is *parallel* to the cylinder axis. Under this condition, a magnetization current $\vec{J}_{ms} = \vec{J}_{ms,l} \hat{l}$ is induced on the cylinder surface, where \hat{l} is a unit vector tangential to the cylinder surface. Taking dot product of \hat{l} with both sides of equation (3), and making use of vector identities, one converts it to

$$\begin{aligned} & \frac{1}{\mu_r} B_{e,z} + \frac{\mu_0}{\mu_r} \lim_{\vec{\rho} \downarrow C} \oint_C \vec{J}_{ms,l}(\vec{\rho}') \frac{\partial G(\vec{\rho}, \vec{\rho}')}{\partial n'} dl' \\ & = B_{e,z} + \mu_0 \lim_{\vec{\rho} \downarrow C} \oint_C \vec{J}_{ms,l}(\vec{\rho}') \frac{\partial G(\vec{\rho}, \vec{\rho}')}{\partial n'} dl' \end{aligned} \quad \vec{\rho} \in C \quad (9)$$

Again, one notes that

$$\frac{\partial G}{\partial n'} = -\frac{1}{2\pi} \frac{\cos \theta'}{|\vec{\rho} - \vec{\rho}'|} \quad (10)$$

in which

$$\cos \theta' = \hat{n}' \cdot \frac{\vec{\rho} - \vec{\rho}'}{|\vec{\rho} - \vec{\rho}'|} \quad (11)$$

Then, going through the limiting procedure [7] similar to that in the previous case, one arrives at

$$\begin{aligned} & -\frac{1}{\mu_r} B_{e,z} + \frac{1}{2\pi} \frac{\mu_0}{\mu_r} \left[\oint_C J_{ms,l}(\vec{\rho}') \frac{\cos \theta'}{|\vec{\rho} - \vec{\rho}'|} dl' - \frac{J_{ms,l}(\vec{\rho})}{2} \right] \\ & = -B_{e,z} + \frac{1}{2\pi} \mu_0 \left[\oint_C J_{ms,l}(\vec{\rho}') \frac{\cos \theta'}{|\vec{\rho} - \vec{\rho}'|} dl' + \frac{J_{ms,l}(\vec{\rho})}{2} \right] \end{aligned} \quad (12)$$

or

$$\frac{\mu_0}{2\pi} \oint_C J_{ms,l}(\vec{\rho}') \frac{\cos \theta'}{|\vec{\rho} - \vec{\rho}'|} dl' + \frac{\mu_r + 1}{\mu_r - 1} \frac{\mu_0 J_{ms,l}(\vec{\rho})}{2} = B_{e,z}(\vec{\rho}), \quad \vec{\rho} \in C \tag{12'}$$

where $\cos \theta'$ is defined in equation (11).

3. NUMERICAL SOLUTION SCHEME

The integral equations (8') and (12') are solved numerically employing the moment method [5]. The cylinder bounding contour C is partitioned into N subcontours ΔC_n and each of them is approximated by a straight line segment of length Δl_n . The unknown magnetization currents $\vec{J}_{ms,z}$ in equation (8') and $\vec{J}_{ms,l}$ in equation (12') are approximated as

$$J_{ms,z}(\vec{\rho}) = \sum_{n=1}^N J_{nl}^{nz} \Pi_n(\vec{\rho}) \tag{13}$$

where J_{nl}^{nz} are the unknown constants to be determined and Π_n is a pulse function defined by

$$\Pi_n(\vec{\rho}) = \begin{cases} 1, & \vec{\rho} \in \Delta C_n, \\ 0, & \text{otherwise.} \end{cases} \tag{14}$$

Replacing the surface current $\vec{J}_{ms,z}$ in equation (8'), corresponding to $\vec{B}_e = \vec{B}_{e,l}$, by its pulse expansion and then using point-matching at subcontour centers located by $\vec{\rho}_m$, one converts the integral equation into a set of N simultaneous equations

$$\sum_{n=1}^N J_{nz} \Gamma_{mn} = B_m, \quad m = 1, 2, \dots, N, \tag{15}$$

where $B_m = B_{e,l}(\vec{\rho})$ and where

$$\Gamma_{mn} = -\frac{\mu_0}{2\pi} \int_{-\Delta l_n/2}^{\Delta l_n/2} \frac{\cos \theta_{mn}}{|\vec{\rho}_m - \vec{\rho}_n - l' \hat{l}_n|} dl' - \frac{\mu_0(\mu_r + 1)}{2(\mu_r - 1)} \delta_{mn} \tag{16}$$

in which $\vec{\rho}_n$ locates the center of ΔC_n , \hat{l}_n is the unit vector along ΔC_n , and δ_{mn} is the Kronecker delta

$$\delta_{mn} = \begin{cases} 1, & m = n, \\ 0, & \text{otherwise.} \end{cases} \tag{17}$$

Also, in equation (16), $\cos \theta_{mn}$ is defined by

$$\cos \theta_{mn} = \frac{(x_m - x_n - \hat{x} \cdot \hat{l}_n l')(\hat{y} \cdot \hat{l}_m) - (y_m - y_n - \hat{y} \cdot \hat{l}_n l')(\hat{x} \cdot \hat{l}_m)}{|\vec{\rho}_m - \vec{\rho}_n - l' \hat{l}_n|} \quad (18)$$

The magnetization current $J_{ms,l}$ in equation (12'), corresponding to $\vec{B}_e = \vec{B}_{e,z}$, can also be determined employing moment method. Going through the same pulse expansion and point matching procedure, equation (12') is converted into a set of N simultaneous equations

$$\sum_{n=1}^N J_{nl} \Gamma_{mn} = B_m \quad m = 1, 2, \dots, N, \quad (19)$$

where $B_m = B_{e,z}(\vec{\rho}_m)$ and where

$$\Gamma_{mn} = \frac{\mu_0}{2\pi} \int_{-\Delta l_n/2}^{\Delta l_n/2} \frac{\cos \theta'_{mn}}{|\vec{\rho}_m - \vec{\rho}_n - l' \hat{l}_n|} dl' + \frac{\mu_0(\mu_r + 1)}{2(\mu_r - 1)} \delta_{mn} \quad (20)$$

in which $\cos \theta'_{mn}$ is defined by

$$\cos \theta'_{mn} = \frac{(x_m - x_n)(\hat{y} \cdot \hat{l}_n) - (y_m - y_n)(\hat{x} \cdot \hat{l}_n)}{|\vec{\rho}_m - \vec{\rho}_n - l' \hat{l}_n|} \quad (21)$$

4. COMPUTATION OF MAGNETIC FIELD

Based on the numerical solution of the magnetization current, \vec{J}_{ms} , on the cylinder surface, the magnetic flux density created by the magnetized cylinder can be determined by

$$\vec{B}_s = -\mu_0 \oint_C \vec{J}_{ms}(\vec{\rho}') \times \nabla G(\vec{\rho}, \vec{\rho}') dl' \quad (22)$$

When the earth's magnetic field is perpendicular to the cylinder axis, the magnetic field is due to a z -directed magnetization current $\vec{J}_{ms,z}$. The two components of the magnetic field are found to be

$$B_x = \mu_0 \oint_C \vec{J}_{ms,z}(\vec{\rho}') \frac{\partial G(\vec{\rho}, \vec{\rho}')}{\partial y} dl' \quad (23a)$$

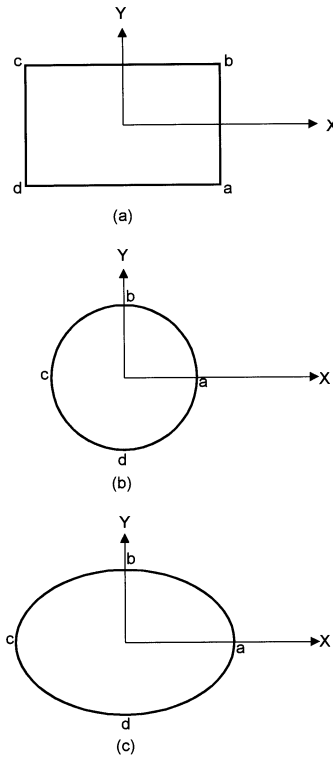


Figure 3. Cylinders of various cross sections. (a) Rectangular cylinder; (b) Circular cylinder; (c) Elliptic cylinder.

and

$$B_y = -\mu_0 \oint_C \vec{J}_{ms,z}(\vec{\rho}') \frac{\partial G(\vec{\rho}, \vec{\rho}')}{\partial x} dl' \tag{23b}$$

or

$$B_x = \mu_0 \sum_{n=1}^N J_{nz} \int_{-\Delta l_n/2}^{\Delta l_n/2} \frac{\partial G(\vec{\rho}, \vec{\rho}')}{\partial y} dl' \tag{23a'}$$

and

$$B_y = -\mu_0 \sum_{n=1}^N J_{nz} \int_{-\Delta l_n/2}^{\Delta l_n/2} \frac{\partial G(\vec{\rho}, \vec{\rho}')}{\partial x} dl' \tag{23b'}$$

When the earth’s magnetic field is parallel to the cylinder axis, the magnetic field produced by the cylinder is due to a circumferential

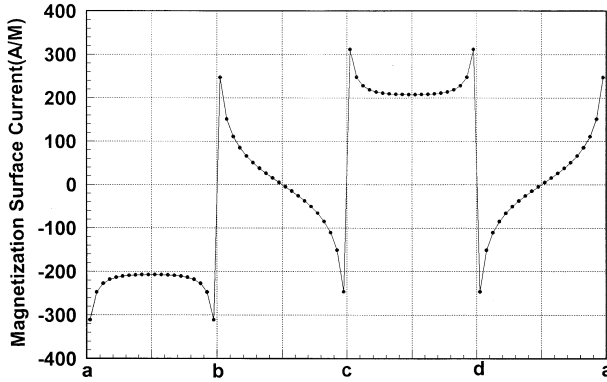


Figure 4. Magnetization current $J_{ms,z}$ on the surface of a rectangular cylinder.

magnetization current. The magnetic field is z -directed and it can be found by

$$\vec{B}_s = -\mu_0 \oint_C \vec{J}_{ms,i} \hat{l}' \times \left(\hat{x} \frac{\partial G(\vec{\rho}, \vec{\rho}')}{\partial x} + \hat{y} \frac{\partial G(\vec{\rho}, \vec{\rho}')}{\partial y} \right) dl' \quad (24)$$

or

$$\vec{B}_s = -\mu_0 \sum_{n=1}^N J_{nl} \int_{-\Delta l_n/2}^{\Delta l_n/2} \hat{l}' \times \left(\hat{x} \frac{\partial G(\vec{\rho}, \vec{\rho}')}{\partial x} + \hat{y} \frac{\partial G(\vec{\rho}, \vec{\rho}')}{\partial y} \right) dl' \quad (24')$$

5. RESULTS AND DISCUSSION

In this section, we first show the numerical results of the magnetization current on a magnetizable cylinder placed in the earth’s magnetic field. Then, data of the magnetic flux density produce by the cylinder are presented. In particular, data of the total magnetic field, as the sum of the magnetic field of the earth and that produced by the cylinder, near the cylinder surface are analyzed and compared with the boundary condition requirements. In the computation, the earth’s magnetic flux density is taken to be 10^{-4} Wb/m^2 (1 Gauss). The relative permeability of the cylinder is assumed to be $\mu_r = 60$. The cylinder may be such oriented that its axis is either parallel or perpendicular to the

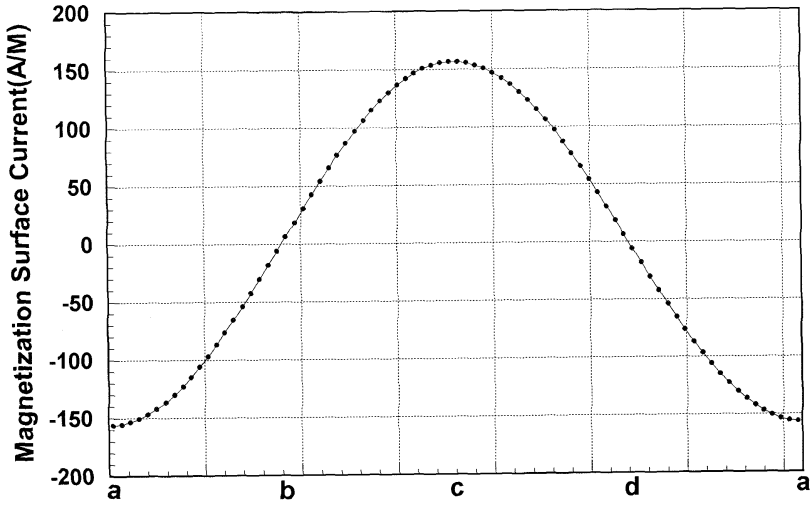


Figure 5. Magnetization current $J_{ms,z}$ on the surface of a circular cylinder.

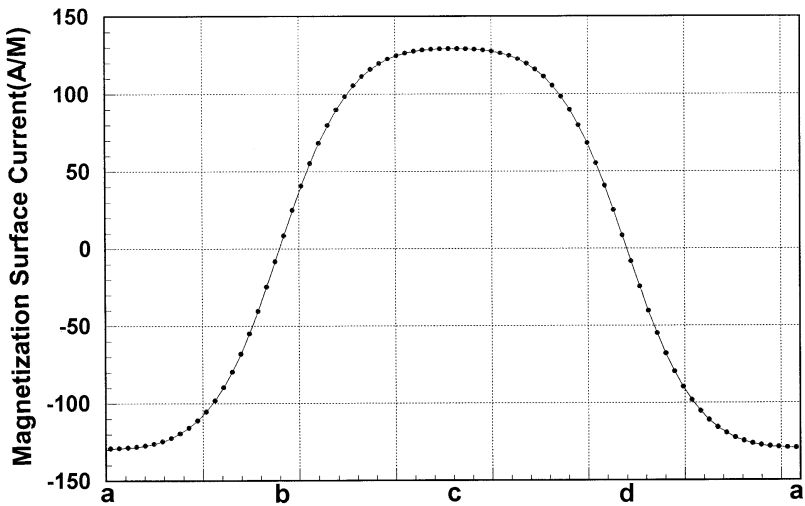


Figure 6. Magnetization current $J_{ms,z}$ on the surface of an elliptic cylinder.

earth's magnetic field. It can be of general cross section. However, data are only presented for a $1m \times 1m$ rectangular cylinder, a circular cylinder of radius $r = 1m$, and an elliptic cylinder with a $1.5m$ major axis and a $1m$ minor axis. The cross sections of the cylinders are displayed in Fig. 3.

In Figs. 4–6 are depicted distributions of magnetization current $J_{ms,z}$ on the surface of a cylinder magnetized in the earth's magnetic field which is perpendicular to the cylinder axis ($\vec{B}_e = B_{e,y}\hat{y}$). Data of magnetization current on the surface of a rectangular cylinder are presented in Fig. 4. The magnetization current has peak values at corners of the rectangular cylinder and the current changes its sign across the corners as one would predict. The data shown in this figure agree with that presented in [3]. In Figs. 5 and 6 are illustrated magnetization currents on the surface of a circular cylinder and an elliptic cylinder. One sees that the magnetization currents change smoothly on the surface of the circular cylinder and elliptic cylinder as expected. In Fig. 7 is displayed the magnetization current $J_{ms,l}$ on the surface of a circular cylinder placed in the earth's magnetic field which is parallel to the cylinder axis ($\vec{B}_e = B_{e,z}\hat{z}$). Because the earth's magnetic field, as the "excitation" field, is tangential to the cylinder surface, and is invariant all along the cylinder bounding contour, one predicts that the magnetization current should be invariant as well. Indeed, the magnetization current shown in Fig. 7 is a constant over the cylinder surface. Since data of the magnetization currents on a rectangular cylinder and on an elliptic cylinder exhibit the similar characteristic, they are not shown in this paper. Further, one notes that equation (12') is analytically solvable for a constant magnetization current $J_{ms,l}$ on a circular cylinder, with the earth's magnetic field parallel to its axis. For the parameters specified in this section, the analytic solution of the magnetization current density is 4,695 A/M, which agrees with the numerical result depicted in Fig. 7.

Based on knowledge of the magnetization current, the magnetic field due to a magnetizable cylinder placed in the earth's magnetic field is calculated. Data of magnitude of the magnetic flux density generated by a circular cylinder and by an elliptic cylinder, with the earth's magnetic field perpendicular to their axes, are presented in Figs. 8 and 9. As one would predict, the magnetic flux density in each case decreases as the distance from the cylinder increases. In Fig. 10 are depicted the numerical results of magnetic flux density produced by

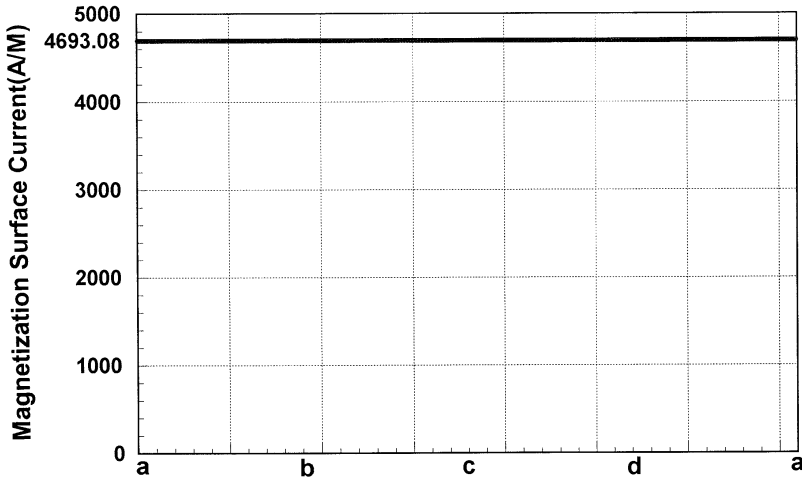


Figure 7. Magnetization current $J_{ms,l}$ on the surface of a circular cylinder.

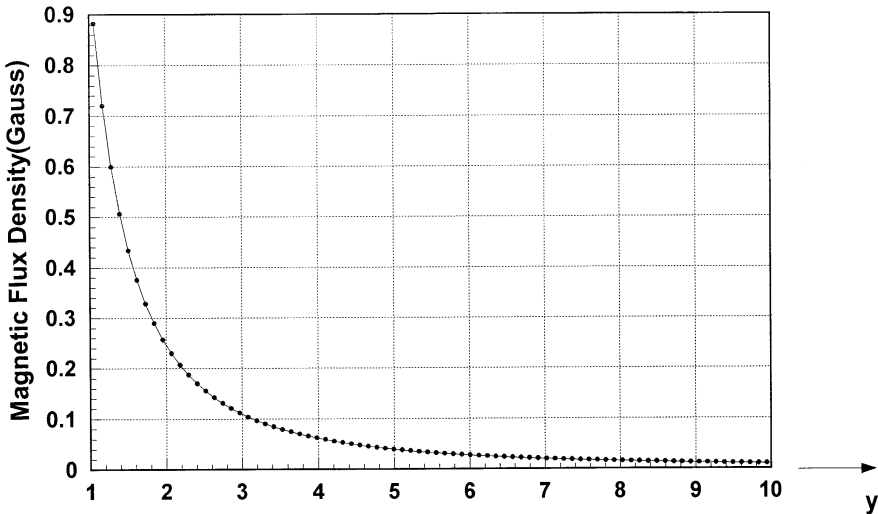


Figure 8. Magnitude of magnetic flux density produced by a circular cylinder, with earth's magnetic field perpendicular to its axis, observed at $x = 0, y = 1 - 10m$.

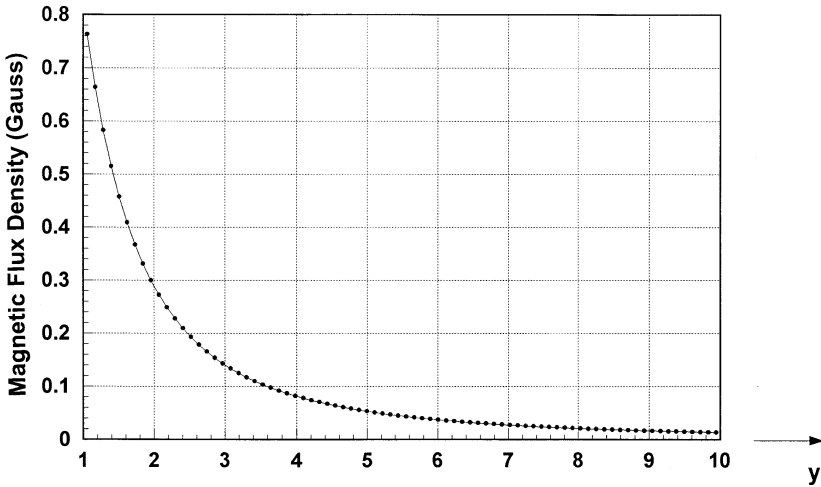


Figure 9. Magnitude of magnetic flux density produced by an elliptic cylinder, with earth's magnetic field perpendicular to its axis, observed at $x = 0, y = 1 - 10m$.

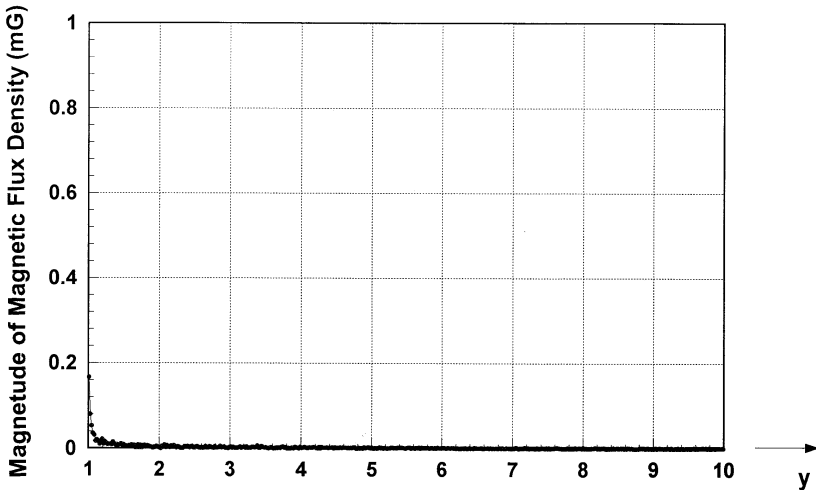


Figure 10. Magnitude of magnetic flux density produced by a circular cylinder, with earth's magnetic field parallel to its axis, observed at $x = 0, y = 1 - 10m$.

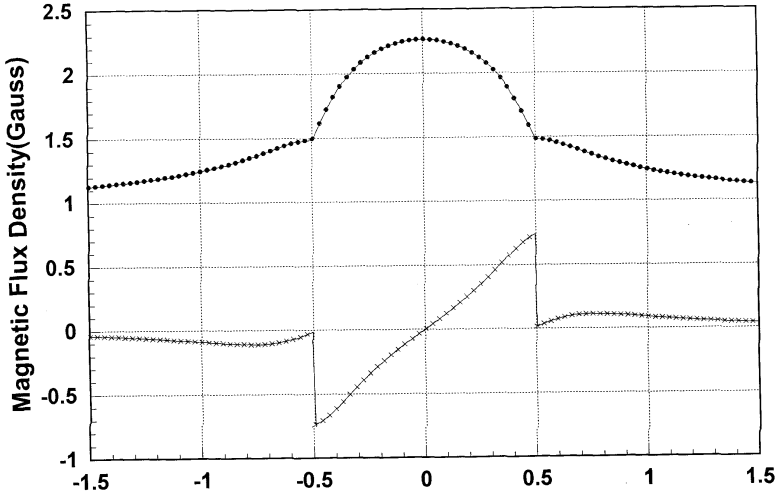


Figure 11. Total magnetic field ($- \times - \times - \times - B_x$, $- \bullet - \bullet - \bullet - B_y$) of a rectangular cylinder, with y -directed earth's magnetic field, observed at $x = 0.25m$, $y = -1.5-1.5m$.

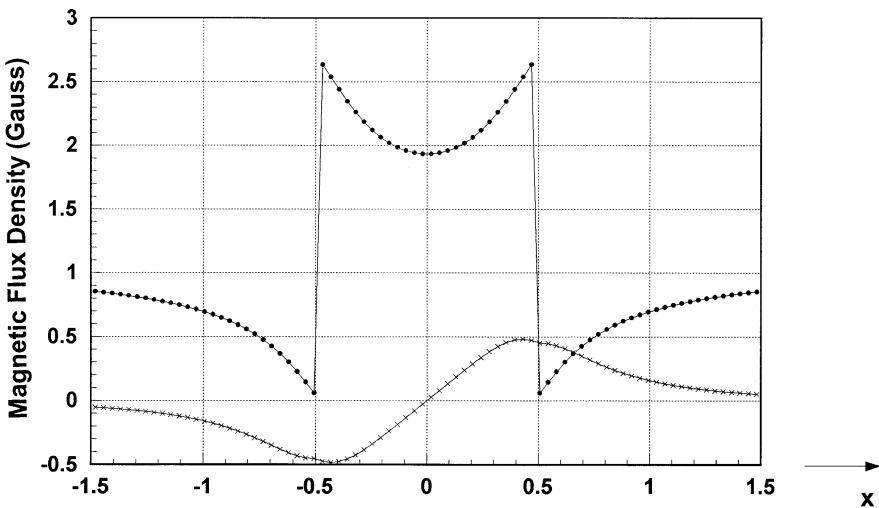


Figure 12. Total magnetic field ($- \times - \times - \times - B_x$, $- \bullet - \bullet - \bullet - B_y$) of a rectangular cylinder, with y -directed earth's magnetic field, observed at $x = -1.5-1.5m$, $y = 0.25m$.

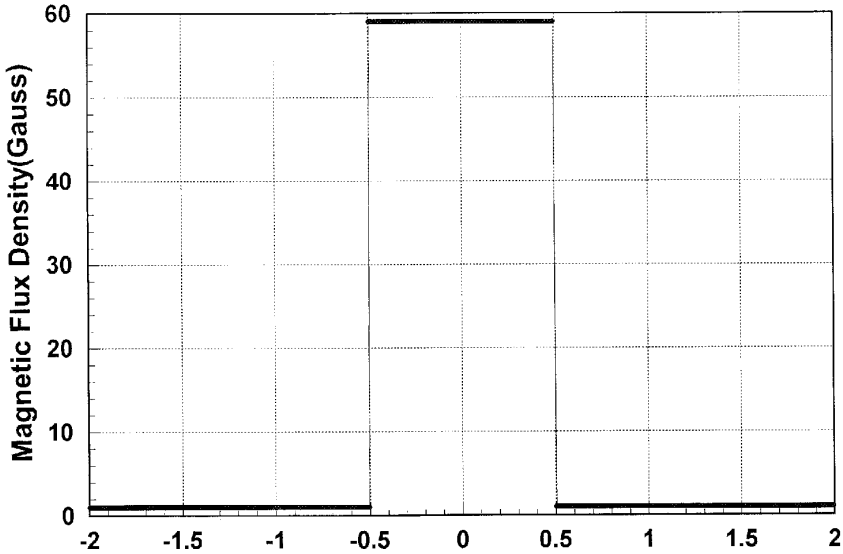


Figure 13. Total magnetic field of a rectangular cylinder, with earth's magnetic field parallel to its axis, observed at $x = -2-2m$, $y = 0.25m$.

a circular cylinder, with the earth's magnetic field parallel to its axis, which is almost zero outside the cylinder. For a rectangular cylinder and an elliptic cylinder, with the earth's magnetic field parallel to their axes, the calculated magnetic flux density due to the cylinder (not presented in this paper) is also almost zero.

To validate the computational method presented in this paper, the numerical results of the total magnetic field, as the sum of the earth's magnetic field and the magnetic field produced by the cylinder, are compared with the boundary condition requirements near the cylinder surface. For convenience of making the comparison, we use the data for a rectangular cylinder as examples. In Figs. 11 and 12 are presented numerical results of x - and y -component of the total magnetic field for a rectangular cylinder, with the earth's magnetic field $\vec{B}_e = B_{e,y}\hat{y}$. Data depicted in Fig. 11 are for the magnetic field observed at $x = 0.25m$ and y varying from $-1.5m$ to $1.5m$. One observes that at $y = \pm 0.5m$, or on the surface of the cylinder, the normal component of the magnetic flux density (B_y) is continuous and the tangential component of the magnetic flux density (B_x) is discontinuous, as required by boundary conditions. The same observation applies to the data presented in Fig. 12, at $x = \pm 0.5m$ where

B_x is the normal component and B_y is the tangential component. In both figures, the ratio of the tangential components of the magnetic flux densities evaluated on the opposite sides of the boundary tends to be equal to the contrast of the permeability of the cylinder and that of the external material, as the observation point approaches to the boundary. When the earth's magnetic field $\vec{B}_e = B_{e,z}\hat{z}$, the total magnetic flux density is also z directed. As one can see from the data displayed in Fig. 13, on the cylinder surface $x = \pm 0.5m$, the z -directed total magnetic flux density, which is tangential to the cylinder surface, is discontinuous. Also, one notes that the ratio of the magnetic flux densities on the opposite sides of the boundary displayed in Fig. 13 is about equal to 60. This value is exactly the same as the relative permeability of the cylinder taken for our computation. This comparison shows that the computed magnetic flux density agrees with that required by the boundary condition.

REFERENCES

1. Brunotte, X., G. Meunier, and J.-P. Bongiraud, "Ship magnetization modeling by the finite element method", *IEEE Trans. on Magnetics*, Vol. 29, No. 2, 1970–1975, March 1993.
2. Lapedes, D. N., ed., *McGraw-Hill Encyclopedia of the Geological Sciences*, New York: McGraw-Hill, 1977.
3. Davey, K. R., "Degaussing with BEM and MFS", *IEEE Trans. on Magnetics*, Vol. 30, No. 5, 3451–3454, September, 1994.
4. *Jane's Fighting Ships*, 1995/96, New York, Franklin Watts.
5. Harrington, R. F., *Field Computation by Moment Method*, Malabar, Florida: Robert E. Krieger Publishing Company, 1982.
6. Lean, M. H., "Application of boundary integral equation methods to electromagnetics", *IEEE Trans. on Magnetics*, Vol. 21, No. 5, 1823–1828, September, 1985.
7. Butler, C. M., D. R. Wilton, and A. W. Glisson, "Fundamentals of numerical solution methods in electromagnetics", *Short Course Notes*, The University of Mississippi, 1982.